Hybrid Membrane/PSA Processes for CO_2/N_2 Separation[†]

Isabel A.A.C. Esteves[*] and José P.B. Mota *Requimte/CQFB, Departamento de Química, Faculdade de Ciências e Tecnologia, Universidade Nova de Lisboa, 2829-516 Caparica, Portugal.*

ABSTRACT: New integrated schemes combining membrane permeation and pressure swing adsorption (PSA) have been developed for gas separation. By using the membrane as a pre-bulk separation unit and coupling it to the intrinsically dynamic periodic operation of the PSA, the separation performance of the hybrid scheme is enhanced with respect to that of the two stand-alone units. Instead of constant-composition regular feed, the PSA is fed with a mixture which is progressively enriched in the more adsorbed component during the pressurization and high-pressure adsorption steps of the cycle. This results in sharper concentration fronts.

The hybrid scheme detailed here has been applied successfully to the bulk separation of an 30:70 mol% CO_2/N_2 mixture over activated carbon. Process performance is reported in terms of product recovery and purity at cyclic steady state. Numerical simulations were validated by experimental work on a composite membrane and a laboratory-scale PSA unit. For the examples studied, product purity and recovery for the hybrid process were increased by 23% and 58% for CO_2, and by 14% and 5% for N_2, compared to an equivalent stand-alone PSA.

1. INTRODUCTION

Extensive efforts have been devoted to developing theories and industrial practices for gas separation by PSA and membrane permeation (Yang 1987; Ruthven *et al*. 1994; Karger and Ruthven 1992; Vu *et al*. 2003; Wind *et al*. 2004). These two technologies are frequently considered as alternatives to the conventional cryogenic process. Their configurations have been widely studied in order either to minimize recompression work to reduce final operational costs, or to give a better re-use to some waste gases that are not usually recovered by conventional methods.

Membrane separation is generally unfavourable when a high-purity product is required and is usually considered to be more suitable for bulk separation. Often, membranes provide a moderately pure product at low cost that may be inexpensively upgraded by a subsequent process (Feng *et al*. 1998; Drioli and Romano 2001; Baker 2002). This fact has motivated active research on the integration of membranes with other separation processes.

Cyclic adsorption processes are well-established separation methods in the chemical and petrochemical industries. Since the pioneering works of Skarstrom (1958) and Guerin de Montgareuil and Domine (1957, 1964) on the pressure swing adsorption (PSA) process, many schemes have been developed and commercialized in order to increase energy efficiency, improve

[†]First presented at the 6th Brazilian Meeting on Adsorption held in Maringá, State of Paraná, Southern Brazil on August 13–16, 2006.

[*]Author to whom all correspondence should be addressed. E-mail: iaesteves@dq.fct.unl.pt; pmota@dq.fct.unl.pt.

product purity and enhance operation flexibility (Tondeur 1985). Although there are some published works on hybrid membrane/PSA systems (Baker 1998; Baker and Kaaeid 2000; Baker *et al*. 2001; Sircar and Ho 1992), truly synergistical concepts have only been proposed by Feng *et al*. (1998), Esteves and Mota (2002, 2003a,b, 2004, 2005, 2007) and Esteves (2005). An important conclusion drawn from these works is that membrane permeation can be an effective aid in the pressurization and high-pressure adsorption steps of a typical PSA process.

The results also indicate the feasibility of incorporating membrane permeation into the blowdown step of the PSA cycle, so that the pressure difference available from the PSA can be used for operating the membrane. Therefore, a complete understanding of integrated processes for gas separation and their commercial availability has not yet been fully realized.

This paper describes novel gas separation processes coupling PSA and membrane permeation. In particular, the performance of one of the proposed hybrid schemes for CO_2/N_2 separation is analyzed for different operating conditions, both experimentally and by process simulations. It is shown that the integrated steps of the hybrid system sharpen the composition wave fronts inside the adsorbent bed, giving rise to a decrease in band broadening and higher product purity, thus enhancing the overall process performance with respect to that of the stand-alone units.

2. PROCESS DESCRIPTION

In our integrated processes the operating pressure of the PSA unit is used as the driving force for permeation, which assists the pressurization (PR) and adsorption (HPA) steps of the PSA process. To fully explore the synergy between both units for a wide range of separation scenarios, two cases have been considered (Figure 1):

- Case A, in which the more permeable component is the least adsorbed.
- Case B, in which the more permeable component is the more adsorbed.

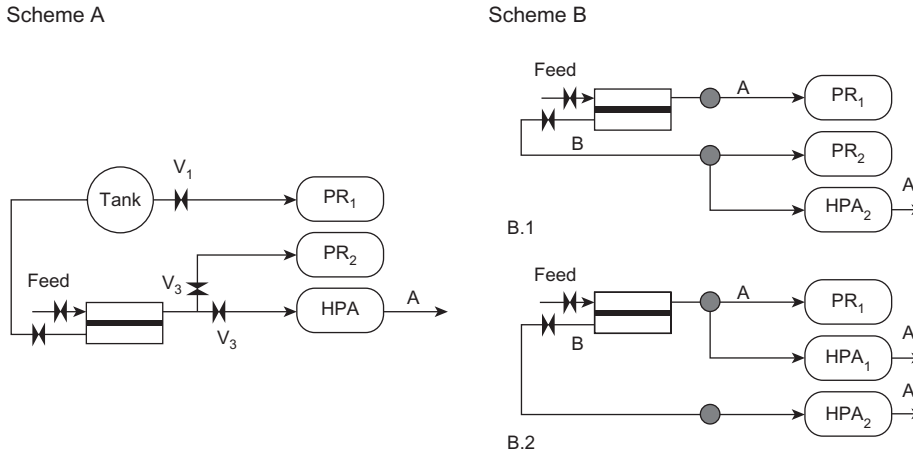

Figure 1. The two hybrid schemes developed (scheme A and scheme B). Cases B.1 and B.2 are the possible operational situations occurring in scheme B. The notation is as follows: PR, pressurization; HPA, high-pressure adsorption; 1 and 2 correspond to the 1st and 2nd step stages, respectively. The product from the HPA step is enriched in the less adsorbed species (A).

Case B is presented here as a method suitable for CO_2/N_2 and CH_4/CO_2 separations, whereas case A has been successfully applied elsewhere for H_2/CH_4 and CH_4/CO_2 separations (Esteves and Mota 2002, 2003a, 2007; Esteves 2005). In both processes, instead of a regular binary feed mixture of A (least adsorbed) and B (more strongly adsorbed), the PSA is fed with a mixture which is progressively enriched in the more adsorbed component during the pressurization and high-pressure adsorption steps of the PSA cycle. Permeate and residue streams are fed to the PSA at different steps of the cycle. A brief process description of each hybrid scheme developed is given next.

In case A, the residue stream is sent directly to the PSA, whereas the permeate stream is stored in an intermediate tank before being sent to the adsorbent unit. The cycle starts with the incomplete pressurization (PR_1) of one of the PSA beds, using the gas stored in the tank which is enriched in the least adsorbed species A. The gas stored in the tank corresponds to a permeate stream that was obtained during the previous high-pressure adsorption (HPA) step operating on the other PSA bed. In step PR_1, valve V_1 is kept open while valves V_2 and V_3 stay closed until pressure equalization between the tank and the bed is established. Then, the tank outlet is closed by shutting V_1. To complete the pressurization step (PR_2), valve V_3 is opened and the bed is pressurized with regular feed gas, which is less rich in species A than the permeate stream employed in step PR_1. During PR_2, the membrane behaves essentially as an empty tube, since both permeate and residue sides are at the feed pressure P_H. Thus, during this step, the residue stream has essentially the same composition as the regular feed.

The cycle then follows with the HPA step that is initiated by opening valve V_2, while feeding the PSA with the residue stream from the membrane at a prescribed flow rate. The residue is enriched in the strongly adsorbed component B, while permeate is stored in the tank to be employed in the next cycle. During HPA, the residue pressure is kept constant at the high-pressure value P_H, whereas the permeate pressure increases with time due to gas build-up in the tank. This happens first through fast equalization between the tank and the permeate side of the membrane and then slowly as more gas is driven through the membrane, while both the permeate side of the membrane and the tank together build up pressure at the same rate. The two pressurization steps, PR_1 and PR_2, as well as the HPA step, are illustrated schematically in Figure 2 (Esteves and Mota 2007).

Ultimately, the PSA cycle proceeds with the following steps: co-current blowdown (HBB) to recover the residual amount of A, which was pushed to the end of the bed during HPA; counter-current blowdown (LBD) and purge (LPG) to recover species B and to regenerate the bed for the next cycle. During these steps the membrane is operating with the other bed in order to provide continuity of flow. Although each bed is operated in batch mode, the system as a whole is a continuous one that is operated in cyclic steady state (CSS). The membrane module behaves similarly because of its coupling to the PSA cycle.

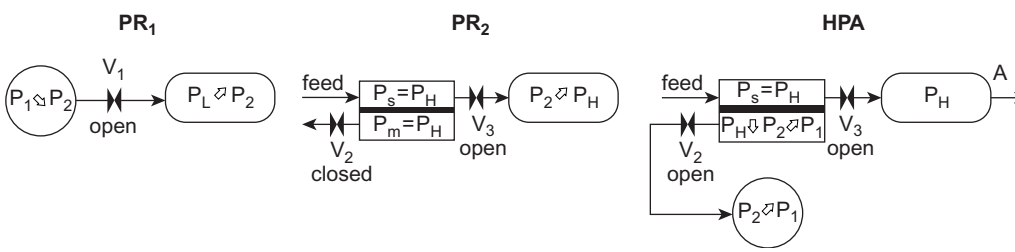

Figure 2. Schematic illustration of the integrated cycle for scheme A: P_1 is the intermediate pressure in the tank after permeation at the end of the HPA step; P_2 represents the equalization pressure at the end of step PR_1. Downward and upward arrows indicate decreasing and increasing pressure changes, respectively.

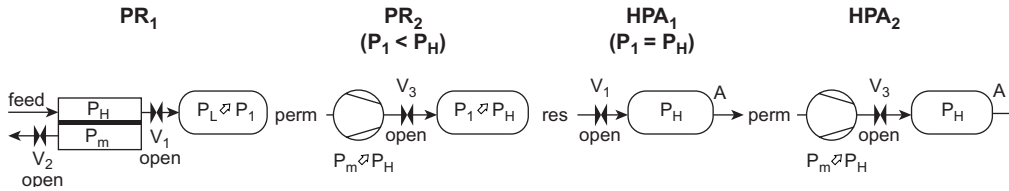

Figure 3. Schematic illustration of the integrated cycle for scheme B: P_1 is the intermediate pressure in the adsorption column after permeation at the end of step PR_1. Upward arrows indicate increasing pressure changes.

Hybrid process B is applicable when the more strongly adsorbed species is also the more permeable one. In this scheme, the pressures on both sides of the membrane are kept constant during permeation. Although the residue stream is sent directly to the PSA, the permeate stream is temporarily stored and can either be used to complete the pressurization step or be sent directly to the bed during the adsorption step. This depends on the range of total feed amount admitted per cycle. For a more comprehensive understanding of this process, a schematic diagram of its cyclic operating principle is given in Figure 3.

The membrane is fed with the binary mixture and a pre-separation is performed by sequentially pressurizing the PSA bed with the residue stream followed by the collected permeate. As in scheme A, the PSA cycle comprises the sequential steps of pressurization, high-pressure adsorption, co- and counter-current blowdowns, possibly followed by a purge step with part of the adsorption product or/and an evacuation at sub-atmospheric pressure.

The integrated cycle starts with a permeation step with the high-pressure side of the membrane at $P_1 = P_H$ and the low-pressure side at $P_2 = P_m$. Here, P_m is an intermediate pressure that must be appropriately selected for each separation because, unlike in process A, the gas coming from the permeate must be re-pressurized to feed the HPA step. Simultaneously, a first pressurization stage (PR_1) takes place with the residue effluent stream from the membrane enriched in A, until pressure equalization between the membrane and the bed is established. Subsequently, two situations can occur:

- If the pressure in the bed is lower then the adsorption pressure, P_H, there is insufficient residue to complete the pressurization step (case B.1), and the bed is pressurized with permeate gas enriched in the more strongly adsorbed species B (step PR_2). After PR_2, the membrane is no longer operational for this PSA bed. The HPA step (HPA_2) is initiated by feeding the PSA with the rest of the permeate obtained from the membrane at a prescribed flow rate. During this stage the permeate pressure is kept constant at P_H.
- If the adsorption pressure is attained during permeation and there is residue left from the membrane (case B.2), the cycle proceeds with an HPA step (HPA_1) using that stream enriched in species A. After HPA_1, the membrane is no longer operational for this bed. The bed pressure is kept at P_H and the high-pressure adsorption step is then completed using the permeate enriched in component B (HPA_2).

The PSA cycle proceeds with co- and counter-current blowdowns, as in case A in which the bed is depressurized co-currently to the feed from P_H to an intermediate pressure P_m and then to P_L counter-currently to the feed. Finally, a low-pressure purge (LPG) at P_L with HPA product may occur to recover species B and to regenerate the bed for the next cycle. It is worth mentioning that scheme B requires a pressurization of the permeate to P_H, prior to being fed to the bed, which increases the power consumption of the system. In this case, performance enhancement has to be evaluated against other potential system costs.

3. THEORETICAL MODEL

For brevity of presentation, we do not reproduce in full detail the model equations and parametric analysis for each scheme developed (Esteves 2005). Instead, we highlight some of the more representative results that demonstrate the hybrid concept and its enhancements relative to the more conventional units.

The governing equations for hybrid process B are summarized in Table 1; the dimensions of the laboratory-scale PSA unit parameters, adsorbent properties, membrane properties and main process simulation parameters are listed in Table 2; Tables 3 and 4 list the boundary conditions. Variables with no subscript refer to gas in the interparticle void space of the packed bed, subscript 'p' denotes adsorbent properties, 'f' denotes feed conditions, and subscripts 'm' and 's' refer to the permeate and residue sides of the membrane, respectively. Symbol v_h denotes the inlet gas velocity in the HPA step, v_g stands for the purge gas velocity, and y_{ig} represents the mole fraction composition of the purge gas which is taken as the average value of the product composition obtained during the final fraction of the HPA step; t_{PR} is the time required to complete the pressurization step; A_{mem} is the permeation area; L_m is the membrane length; and A_mL_m and A_sL_m are the volumes of the permeate and residue sides of the membrane, respectively. The quantity F_m is used as a scaling parameter for the membrane that represents A_{mem} in dimensionless form by establishing a ratio between a hypothetical molar flow of a pure stream of species A through the membrane unit, when the pressure differential is P_H, P_L, and F_{HPA} is the molar flow through the PSA unit during the HPA step. The reader is referred to the Notation section below for definitions of the other symbols given in Tables 1–4.

To simplify the computational model, the following assumptions have been made: ideal gas behaviour, counter-current flow with negligible pressure change and temperature gradients in the membrane; constant component permeances; a non-isothermal and variable-velocity axially dispersed plug-flow model with negligible pressure loss inside the PSA bed; mass transfer inside the adsorbent particles governed by a pore- and surface-diffusion model (Yang and Doong 1986); thermal equilibrium between the fluid and the particles. Constant physical properties are also assumed for the adsorbates. The integrated model is implemented and solved in gPROMS, which is an established software package for the modelling and simulation of lumped- and distributed-parameter process models with combined discrete and continuous characteristics (Barton and Pantelides 1994; Oh and Pantelides 1996).

The PR step continues until the bed pressure reaches P_H or until the amount of permeate is depleted. The PG step stops when the inlet condition imposed by both v_g and the purge amount is satisfied. Note that the simulation code automatically detects when the feed amount admitted per cycle is insufficient to pressurize the bed up to P_H, and gives an error message.

The pressurization of the PSA bed with residue (PR_1) and permeate streams (PR_2) is assumed to be governed by non-linear pressure dynamics dependent on the feed velocity profile imposed. During the two blowdown (CD and BD) steps, the pressure follows a decaying curve determined experimentally, which can be defined as:

$$\frac{dP}{dt} = \alpha + 2\beta\left(t - t_{ref}\right) + 3\gamma\left(t - t_{ref}\right)^2, \quad 0 < t < t_{CD}, \text{for CD}$$

$$\frac{dP}{dt} = \frac{-\left[\beta + 2\gamma\left(t - t_{ref}\right) + 3\delta\left(t - t_{ref}\right)^2 + 4\zeta\left(t - t_{ref}\right)^3\right]}{\alpha + \beta\left(t - t_{ref}\right) + \gamma\left(t - t_{ref}\right)^2 + \delta\left(t - t_{ref}\right)^3 + \zeta\left(t - t_{ref}\right)^4}, \quad 0 < t < t_{BD}, \text{for BD} \tag{1}$$

with $t_{ref}^{CD} = \Delta t_{PR} + \Delta t_{HPA}$, $t_{ref}^{BD} = \Delta t_{PR} + \Delta t_{HPA} + t_{CD}$, and the $(\alpha, \beta, \gamma, \delta, \zeta)$ parameters are obtained from the fitting of each pressure profile at the specified operating conditions.

TABLE 1. Model Equations for PSA and Membrane Units

Membrane unit	k = m (+), s (–); i = A, B
Permeation fluxes	$N_{i,s\to m} = \wp\left(y_{is}P_s - y_{im}P_m\right), \quad N_{s\to m} = \sum_i N_{s\to m}$
Scaling parameter	$F_m = \wp_B A_{mem}\left(P_H - P_L\right)/F_{HPA}$
Overall material balance	$\frac{\partial P_k}{\partial t} + \frac{\partial\left(v_k P_k\right)}{\partial z} = \pm\frac{A_{mem}RT_f}{A_k L_m}N_{s\to m}$
Component material balance	$\frac{\partial\left(y_{ik}P_k\right)}{\partial t} + \frac{\partial\left(v_k y_{ik}P_k\right)}{\partial z} = \pm\frac{A_{mem}RT_f}{A_k L_m}N_{i,s\to m}$
PSA unit	i = A, B
Overall material balance	$\frac{\partial}{\partial t}\left(\frac{P}{T}\right) + \Omega_P\frac{\partial\bar{q}}{\partial t} + \frac{\partial}{\partial z}\left(\frac{vP}{T}\right) = 0, \quad \bar{q} = \sum_i^n \bar{q}_i$
Component material balance	$\frac{\partial}{\partial t}\left(\frac{Py_i}{T}\right) + \Omega_P\frac{\partial\bar{q}_i}{\partial t} + P\frac{\partial}{\partial z}\left(\frac{y_i v}{T} - \frac{D_L}{T}\frac{\partial y_z}{\partial z}\right) = 0$
Adsorption kinetics	$\frac{\partial\bar{q}_i}{\partial t} = k_i\left(q_i^* - \bar{q}_i\right)$
Sips isotherm model	$q_i^* = \frac{q_{mi}\left(B_i y_i P\right)^{1/n_i}}{1 + \sum_{i=1}^n\left(B_i y_i P\right)^{1/n_i}}, \quad B_i = \frac{b_{0i}}{\eta_i}\exp\left[\frac{Q_i}{RT_{0i}}\left(\frac{T_{0i}}{T} - 1\right)\right],$ $1/n_i = 1/n_{0i} + \alpha_i\left(1 - T_{0i}/T\right)$
Energy balance	$\left(\sum_{i=1}^n y_i C_{pg} - R\right)\frac{\partial P}{\partial t} + \Omega_P\left(C_{pg}\bar{q} + C_{ps}\right)\frac{\partial T}{\partial t} + C_{pg}P\frac{\partial v}{\partial z}$ $+ \Omega_P\sum_{i=1}^n\left(y_i C_{pg}T - H_i\right)\frac{\partial\bar{q}_i}{\partial t} - D_h R\frac{\partial^2 T}{\partial z^2} = \frac{2Rh_w}{\varepsilon R_c}\left(T_w - T\right),$ $H_i = Q_i - \alpha_i RT_{0i}n_i^2\ln\left(\frac{\theta}{1-\theta}\right), \quad \theta = \sum_i q_i/q_i^\infty$
Dispersion coefficients[a]	$D_L = \gamma_1 D_m + \gamma_2 d_p v, \quad D_h = D_h^o + \gamma_3 d_p C_{pg} cv$
Wall energy balance	$\rho_w C_{pw}\frac{\partial T_w}{\partial t} = k_w\frac{\partial^2 T_w}{\partial z^2} + \frac{h_w}{e_w}\left(T - T_w\right)$

[a]Yang (1987); Ruthven *et al*. (1994); Sladek *et al*. (1974); Funazkri and Wakao (1978); Haller *et al*. (1973); $\Lambda_p - \varepsilon_p/(1-\varepsilon)/\varepsilon$; $\Omega_P = \Lambda_p\rho_p R/\varepsilon_p$.

TABLE 2. Parameters for CO_2/N_2 Separation Using Hybrid Process B

Adsorbent and PSA column			
Intraparticle porosity, ε_p	0.656	Wall	
Interparticle porosity, ε	0.476	Thickness, ε_w (mm)	9.50
Particle density, ρ_p (g/cm^3)	0.763	Density, ρ_w (g/cm^3)	8.221
Particle hydraulic radius, r_p (mm)	1.668	Heat capacity, C_{pw} [cal/(g K)]	0.110
Mean pore radius, r_μ (Å)	12.82	Conductivity, k_w [W/(m K)]	43.30
Bed length, L_b (cm)	40–60	Heat-transfer coefficient, h_w [W/(m K)]	63.20
Bed radius, r_b (cm)	1.60		
Sips adsorption isotherm model[a]			
Loading at saturation: q_{m,N_2} (mol/kg)	11.282	q_{m,CO_2} (mol/kg)	20.608
Heterogeneity parameter: n_{0,N_2}	1.140	n_{0,CO_2}	1.252
Exponent parameter: α_{N_2}	0.383	α_{CO_2}	0.126
Affinity coefficient at T_0: b_{0,N_2} (bar^{-n})	0.018	b_{0,CO_2} (bar^{-n})	0.036
Interaction parameter: η_{N_2}	1.04	η_{CO_2}	0.76
Reference temperature: T_{0,N_2} (K)	288.2	T_{0,CO_2} (K)	299.1
Heat of adsorption: Q_{N_2} (kJ/mol)	8.974	Q_{CO_2} (J/mol)	19.583
Membrane unit			
Cross-section relation	$V_k = 0.1V_{PSA}$	Membrane selectivity, α_{CO_2/N_2}	34.4
Permeation area, A_{mem} (m^2)	0.14–0.82	CO_2 permeance, $\wp_{CO_2}$ (GPU)	30.3
Operating parameters range			
Feed pressure, P_H (bar)	6–12	Feed temperature, T_f (K)	299–319
Purge pressure, P_L (bar)	0.34–0.44	Feed composition, y_{if} (%)	30; 50; 80
P/F ratio	0.0–0.8	Feed amount per cycle (ℓ STP)	20.6–180.6
HBD pressure, P_{HBD} (bar)	2.5–5.5	LBD pressure, P_{LBD} (bar)	1.0–2.0
Feed amount per cycle (ℓ STP)	20.6–180.6	Dispersion parameters[b], $\gamma_1, \gamma_2, \gamma_3$	0.7, 0.5, 0.75

[a] Esteves *et al*. (2008) [$r^2 > 0.999$, 0.011 FSE (N_2), 0.013 FSE (CO_2), residuals < 0.04 mol/kg)]. [b] Yang (1987); Funazkri and Wakao (1978).

For the membrane unit, the initial conditions (t = 0) are:

$$P_s = P_H; \quad P_m = P_L; \quad y_{is} = y_{im} = y_{if}; \quad \forall z \in [0, L_m] \tag{2}$$

As far as the PSA unit is concerned, modelling starts with the column filled with the inert or weakly adsorbed component at P_L and a feed temperature of T_f. Experimentally, this was ensured by a constant volumetric feed flow of the inert or less adsorbable component at the beginning of the runs. The initial conditions, at t = 0, are:

$$P = P_L; \quad T = T_f; \quad y_A = 1 \quad y_B = 0, \quad \forall z \in [0, L] \tag{3}$$

$$q_i = q_i^*(T_f, y_A P_L, y_B P_L) \quad \forall z \in [0, L] \tag{4}$$

TABLE 3. Boundary Conditions and Pressure Dynamics Applicable to the PSA Model for Each Step of Hybrid Scheme B[a]

Step	z = 0	z = L	dP/dt
PR_1	$T = T_f, y_i = y_{is}\big\|_{z=L_m}, v = \frac{A_s P_H}{A\varepsilon P} v_s\big\|_{z=L_m}$	$v = 0, T' = 0, y_i' = 0$	–
PR_2[b]	$T = T_f, y_i = y_{im}^{out}, v = \frac{A_m P_H}{A\varepsilon P} v_{PR}$	$v = 0, T' = 0, y_i' = 0$	–
HPA_1	$T = T_f, y_i = y_{is}\big\|_{z=L_m}, v = v_h$	$T' = 0, y_i' = 0$	0
HPA_2	$T = T_f, y_i = y_{im}^{out}, v = v_h$	$T' = 0, y_i' = 0$	0
CD	$T' = 0, y_i' = 0, v = 0$	$T' = 0, y_i' = 0$	equation (1)
BD	$T' = 0, y_i' = 0$	$v = 0, T' = 0\ y_i' = 0$	equation (1)
PG	$T' = 0, y_i' = 0$	$v = -v_g, T = T_f, y_i = y_{ig}$	0

[a]Primed variables denote partial derivatives with respect to the axial coordinate along the packed bed, e.g. $T' \equiv \partial T/\partial z$. Note: inlet conditions (z = 0) for PR, HPA and outlet conditions (z = L) for PG were actually implemented using the Robin-type boundary conditions (equality of mass or heat fluxes at boundary). [b]$v_{PR} = v_h P_H/P$.

TABLE 4. Boundary Conditions Applicable to the Membrane Module for Each Step of Hybrid Scheme B[a]

Step	Stream	z = 0	$z = L_m$
PR_1	Residue	$y_{is} = y_{if}$	$v_s = v_{PR}, y_{is}' = 0$
	Permeate	$y_{im}' = 0$	$v_m = 0, y_{im}' = 0$
PR_2	Residue	$y_{is}' = 0$	$v_s = 0, y_{is}' = 0$
	Permeate	$y_{im}' = 0$	$v_m = 0, y_{im}' = 0$
HPA_1	Residue	$y_{is} = y_f$	$A_s v_s P_s = A\varepsilon v\big\|_{z=0} P, y_{is}' = 0$
	Permeate	$y_{im}' = 0$	$v_m = 0, y_{im}' = 0$
HPA_2	Residue	$y_{is}' = 0$	$v_s = 0, y_{is}' = 0$
	Permeate	$y_{im}' = 0$	$v_m = 0, y_{im}' = 0$
CD, BD, PG	state variables are frozen until next cycle		

[a]Primed variables denote partial derivatives with respect to the axial coordinate along the membrane unit, e.g. $y_{im}' = \partial y_{im}/\partial z$.

The performance of the hybrid process is measured in terms of product purity (Pur) and recovery (Rec), which are defined as follows:

$$Pur_A = \frac{N_{A,out} \text{ in } (HPA + HPB) - N_{A,in} \text{ in LPG}}{N_{A+B,out} \text{ in } (HPA + HPB) - N_{A+B,in} \text{ in LPG}} \quad (5)$$

$$\mathrm{Rec_A} = \frac{\mathrm{N_{A,out}\ in\ (HPA + HPB)} - \mathrm{N_{A,in}\ in\ LPG}}{\mathrm{N_{s,A,in}\ in\ (PR + HPA)}} \tag{6}$$

$$\mathrm{Pur_B} = \frac{\mathrm{N_{B,out}\ in\ (LBD + LPG)}}{\mathrm{N_{A+B,out}\ in\ (LBD + LPG)}} \tag{7}$$

$$\mathrm{Rec_B} = \frac{\mathrm{N_{B,out}\ in\ (LBD + LPG)}}{\mathrm{N_{s,B,in}\ in\ (PR + HPA)}} \tag{8}$$

Both purities and recoveries are volume-averaged quantities, since the composition and effluent flow rates from the PSA bed vary with time. The purge amount is defined as the amount of high-pressure product A used to purge the bed in the purge step,

$$\%\,\mathrm{PG} = \frac{\mathrm{N_{A,in}\ in\ LPG}}{\mathrm{N_{A,out}\ in\ HPA}} \tag{9}$$

4. EXPERIMENTAL

The adsorbent employed in the experiments is a coal-based, high-activity (109% CTC), extruded carbon (2 mm diameter pellets) courtesy of Sutcliffe Speakman Carbons Ltd. (U.K.). The pore structure of the carbon was characterized via nitrogen adsorption at 77 K and mercury porosimetry at room temperature (Esteves *et al*. 2008). A few structural parameters for this carbon are listed in Table 2.

The adsorption equilibria measurements of N_2 and CO_2 on activated carbon were performed using a standard static gravimetric method with real-time acquisition of temperature, pressure and weight of the adsorbent sample. The data for N_2 were obtained at 288.2 K, 310.5 K and 323.4 K, whereas those for CO_2 were taken at 299.1 K, 310.2 K and 319.2 K. The experimental data for the given adsorbates revealed no hysteresis and no significant irreversible loss of carbon capacity upon application of mildly heated vacuum conditions. Further details of these measurements are reported elsewhere (Esteves 2005; Esteves *et al*. 2008).

The Sips isotherm extended to multi-component adsorption was employed to fit the experimental equilibrium data (Table 2). This model has a Langmuirian form when applied to non-uniform surfaces and has been used extensively to model gas adsorption on microporous adsorbents and PSA systems (Yang 1987; Ruthven *et al*. 1994). In order to determine the isotherm parameters for each adsorbate, the experimental adsorption data were fitted using a Matlab script file (isofit2.m) written by Do (1994). This file allows the optimal parameters to be obtained for various adsorption isotherm models, by fitting them simultaneously with data obtained at multiple temperatures. A global isotherm was obtained for each species as illustrated in Figure 4. As expected, the adsorption isotherms exhibit a monotonically concave shape and are type 1 according to the IUPAC classification.

The PSA unit used was built in-house, being a single-column set-up operated automatically. The column itself consists of a variable-length stainless steel (SS) cylinder, the axial position of the temperature sensors located on the inside being adjustable and dependent on the bed length considered. A ca. 30–40 mm height of SS solid spheres, a 2 mm SS perforated plate and a thin

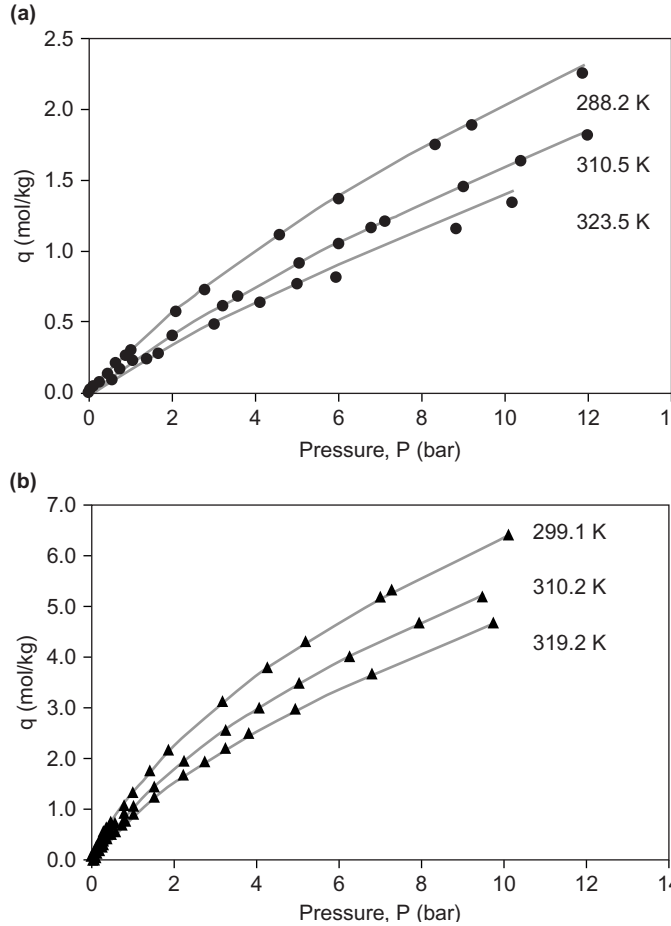

Figure 4. Fitting of the experimental adsorption data for (a) N_2 and (b) CO_2 by the Sips isotherm model whose parameters are listed in Table 2. The symbols represent experimental data while the lines depict the isotherm model.

cotton film acting as a filter were placed at both ends of the column. This procedure ensured a suitable gas distribution through the adsorbent bed and avoided the loss of adsorbent particles. The column was sealed by Teflon rings.

The unit is equipped with platinum Pt100 temperature probes coupled with digital controllers, with temperature maintenance achieved via shielded electrical cables wound around the main section of the apparatus. The feed line is equipped with two mass-flow controllers (0–10, 0–5 or 0–0.1 slpm in N_2, ±1% full scale accuracy); the outlet line has a back-pressure regulator (3–16 bar of controlled pressure with 0.5% accuracy); and in-line there is also a pressure transducer with a linear response of 0–35 bar and ±0.04% full scale accuracy. Several solenoid electric valves ensure the unit operation. Composition analysis is performed by mass spectrometry (MS). All gases used were provided by Air Liquide, Portugal. The system is automated and controlled by Labview software.

A five-step PSA cycle was developed for the separation of CO_2/N_2 mixtures: pressurization (PR) with feed, high-pressure adsorption (HPA), co-current blowdown (HBD), counter-current

blowdown (LBD) and low-pressure purge (LPG). The N_2 product was obtained during HPA and HBD, while CO_2 was produced during LBD and LPG. The PSA model was validated against experimental runs and subsequently employed to study process performance in terms of product purity and recovery. Temperature, gas- and adsorbed-phase concentration profiles, and velocity profiles along the PSA bed were analyzed, as well as the dynamic behaviour histories of these variables during the PSA cycle and until the periodic steady-state was attained (Esteves and Mota 2007). In order to confirm the enhanced performance of the hybrid process, a CO_2/N_2 separation using the hybrid scheme was modelled employing the same conditions as used in the experimental runs.

A typical cellulose acetate membrane with a selectivity of 12–15 under normal operating conditions was employed in the studies reported. This type of membrane is now being slowly replaced by polyimide- and polyaramide-type membranes with selectivities of 20–25 (Baker 2002; Sircar and Ho 1992). For the particular separation reported here, the experimental permeation studies for CO_2 and N_2 were performed in a composite PES/PI (polyethersulphone Sumikaexcel/ polyimide Matrimid 5218) hollow-fibre membrane (Kapantaidakis *et al*. 1996, 2002). The single-component permeances were measured using a standard variable-pressure method and the binary ratios converted into the corresponding ideal selectivities. A specified feed pressure was applied to the shell-side, whereas the permeate side was initially under vacuum. Permeation rates were calculated from the pressure increase as a function of time in a calibrated volume placed on the permeate side of the membrane. Permeation ceased when the pressures on both sides of the membrane were equal. The main physical properties of the membrane are listed in Table 2.

5. RESULTS AND DISCUSSION

5.1. Breakthrough and blowdown experiments

Several breakthrough experiments followed by complete desorption were performed to determine the adsorption kinetics, dispersion effects and heat transfer. In each experiment, the column response at the outlet was analyzed after a step change in the composition of the feed mixture. Once the column was saturated, it was purged with inert carrier until complete desorption was attained.

The adopted formulation for adsorption kinetics is based on the lumped solid-diffusion version of the linear-driving-force (LDF) model (see Table 1), comprising Knudsen and surface-diffusion mechanisms. This model is discussed below. The temperature-independent parameters intervening in the LDF coefficients were determined by fitting several breakthrough and blowdown experiments obtained under diluted conditions where the column behaved isothermally. Once the LDF coefficients were established, the wall heat-transfer coefficient, h_w, was determined from non-isothermal experiments obtained at higher adsorbate concentrations.

The binary mixtures studied were CO_2/He, N_2/He and CO_2/N_2. Several flow rates ranging from 0.84 slpm to 5.05 slpm (STP: 273 K, 1 atm), pressures of 5 and 10 bar, and temperatures of 299, 309 and 319 K (± 1 K) were employed. Seven feed compositions were tested: 0.7, 6, 14, 30, 50, 70 and 80 v/v% while the reproducibility was assessed by repeating some of the experimental runs. The flow rates were sufficiently high to assume negligible fllm mass-transfer resistance.

Figure 5 gives a typical example of a fitted breakthrough curve and its comparison with the experimental measurements. The data depicted were obtained at a high CO_2 loading; under these circumstances, the temperature effects in the bed due to CO_2 adsorption/desorption could not

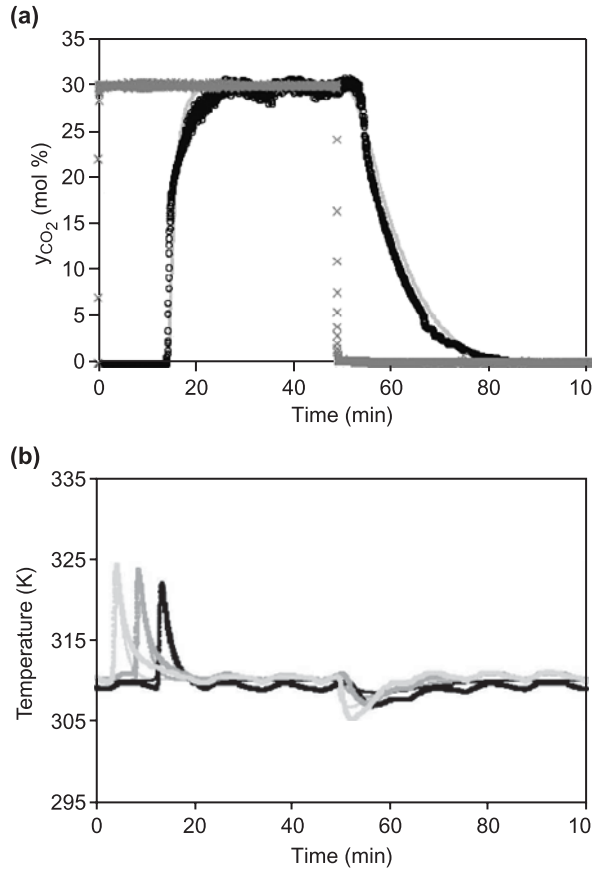

Figure 5. Illustrative breakthrough experiment followed by complete desorption for CO_2/He 30:70 v/v% at 310 K, 5 bar and a total feed flow rate of 3.0 slpm (STP: 273 K, 1 atm): (a) CO_2 temporal profiles at the PSA inlet and exit streams; (b) temperature histories inside the column for (from left to right) the bottom, middle and top of the column, respectively. Symbols represent experimental data and lines are model predictions.

be neglected. It can be seen that the model gives a reasonable description of the breakthrough curve, as well as of the subsequent desorption curve. An average value of 63.2 W/(m^2 K) was obtained for the wall heat-transfer coefficient.

As stated above, the formulation adopted for adsorption kinetics was based on the lumped solid-diffusion version of the LDF model (see Table 1), comprising Knudsen and surface-diffusion mechanisms. With this assumption, the LDF coefficient, k_i, can be expressed as:

$$k_i = k_{iS} + \frac{k_{iK}}{\rho_p\left(\partial q_i^*/\partial c_i\right)} = \frac{15\varepsilon_p}{\tau_p r_p^2}\left[D_{iS} + \frac{D_{iK}}{\rho_p\left(\partial q_i^*/\partial c_i\right)}\right] \tag{10}$$

where ε_p, r_p and τ_p are, respectively, the porosity, radius and tortuosity of the adsorbent particle, and:

$$D_{iK} = 9.7 \times 10^{-9} r_\mu \sqrt{T/M_{iw}}, \quad D_{iS} = D_{io} e^{-E_i/RT} \tag{11}$$

are the Knudsen (m^2/s) and surface-diffusion coefficients; here, r_μ (Å) is the average pore radius, M_{iw} (g/mol) is the molecular weight of the adsorbate, T (K) is the system temperature and E_i is the activation energy for surface diffusion.

For modelling purposes, the value of k_i for N_2 was determined assuming that, as a first approximation, surface diffusion is the predominant contribution to the LDF coefficient. This assumption turned out to be correct as will be shown below. Sladek *et al*. (1974) have developed a general correlation for estimating the surface diffusivity based on the isosteric heat of adsorption and on the type of adsorbent–adsorbate interaction. Using this correlation, the diffusivity ratio D_{N_2}/D_{CO_2} was estimated and employed to determine the LDF coefficient for N_2 from the experimental LDF coefficient for CO_2 at the same temperature, i.e. $k_{N_2} = k_{CO_2}D_{N_2}/D_{CO_2}$. Table 5 and Figure 6 show the results obtained using this approximation and illustrate the temperature dependence of the diffusion coefficients.

Table 6 shows the Knudsen and surface-diffusion contributions to the LDF coefficient obtained for CO_2 and N_2. The Knudsen contribution [i.e. the second term on the right-hand side of

TABLE 5. Intraparticle Diffusion Coefficients for N_2 and CO_2 at 299, 309 and 319 K[a]

$10^3/T$ (1/K)	$10^{-7}D$ (m^2/s)	
	N_2	CO_2
3.34	5.06	0.90
3.23	6.52	1.30
3.13	8.34	2.00
D_o (m^2/s)	1.50×10^{-3}	1.59×10^{-2}
E (kJ/mol)	19.808	30.092

[a]The D_{CO_2} values were determined by fitting the LDF model to CO_2/He breakthrough and blowdown experiments under dilute CO_2 concentration (0.7 v/v%); the D_{N_2} values were determined from the diffusivity ratio, D_{N_2/CO_2}, estimated by the correlation of Sladek *et al*. (1974).

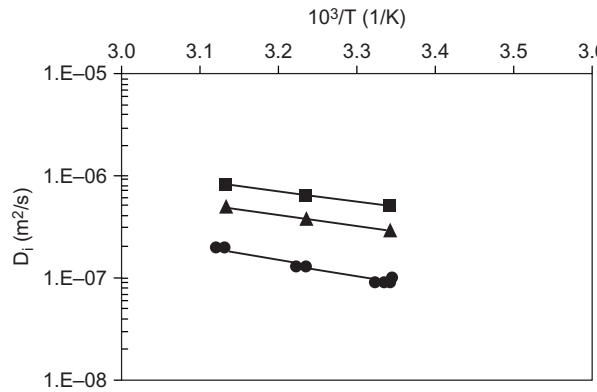

Figure 6. Arrhenius plot showing the temperature dependence of the intraparticle diffusivities for CO_2 (●), N_2 (■) and CH_4 (▲) on the carbon sample.

TABLE 6. Knudsen [$k^*_{iK} = k_{ik}/\rho_p\ (\partial q^*_i/\partial c_i)$] and surface ($k_{iS}$) Diffusion Contributions to the Lumped Solid-diffusion LDF Coefficent [equation (10)] for the CO_2/He and CO_2/N_2 Systems at each Experimental Temperature Studied[a]

Mixture	v/v%	T (K)	CO_2		N_2	
			k_{iS}	$10^3 k^*_{iK}$	k_{iS}	$10^3 k^*_{iK}$
CO_2/N_2[b]	30:70	310.0	0.114	0.832	0.571	5.63
	50:50	309.6	0.114	1.073	0.573	4.67
	80:20	310.6	0.113	1.501	0.573	3.70
CO_2/He	0.7:99.3[c]	299.8	0.079	0.202	–	–
		310.0	0.115	0.209	–	–
		319.4	0.177	0.213	–	–
	30:70[d]	310.1	0.114	0.497	–	–
	30:70[e]	298.9	0.079	0.619	–	–
		310.2	0.114	0.621	–	–
		320.5	0.176	0.624	–	–
	50:50[e]	300.8	0.079	0.768	–	–
		310.3	0.114	0.741	–	–
		319.8	0.176	0.767	–	–
	80:20[e]	299.2	0.079	0.989	–	–
		320.0	0.176	0.979	–	–

[a]Both contributions are expressed in s^{-1}. Runs at [b]10.0 bar and 5.0 slpm, [c]4.0 bar and 1.1 slpm, [d]5.0 bar and 1.4 slpm, and [e]10 bar and 2.7 slpm.

equation (10)], is easily determined from the slope of the adsorption isotherm if reasonable estimates of τ_p and r_μ are known; the surface contribution, k_{iS}, is obtained by difference from equation (10). It is clearly seen that the predominant contribution to intraparticle diffusion results from the surface diffusivity term.

5.2. PSA versus hybrid process

A typical experimental PSA cycle of ca. 14 min was implemented for CO_2/N_2 separation. The periodic cycle comprised five steps: (1) PR up to $P_H = 6$ bar; (2) HPA at P_H; (3) HBD down to $P_m = 3.2$ bar; (4) LBD down to $P_L = 0.3$ bar; (5) and LPG at P_L. During HPA and HBD, N_2 product is obtained, while during LBD and LPG, CO_2 is produced. In order to confirm the enhancement in performance of the hybrid process, this system was modelled both as a conventional PSA process and as an equivalent hybrid unit under exactly the same experimental operating conditions. Both models required ca. 11 cycles to attain the CSS regime. This suggests that adding the membrane module does not slow down the convergence to cyclic steady state.

In general, for the stand-alone process and depending on the feed composition and amount of feed admitted per cycle, the CO_2 purities and recoveries were in the ranges 54–92% and 83–99%, respectively; for N_2, the purities and recoveries were 51–99% and 66–69%, respectively. Figure 7 shows an illustrative comparison between the predicted and the experimental pressure and CO_2 effluent composition histories obtained for a typical PSA run at CSS. The good agreement between the experimental and simulated results strongly supports our stand-alone PSA model.

In order to validate the hybrid concept, two experimental runs, one for the standalone PSA (run A) and another for the integrated process (run B), were performed for CO_2/N_2 separation. Figure 8

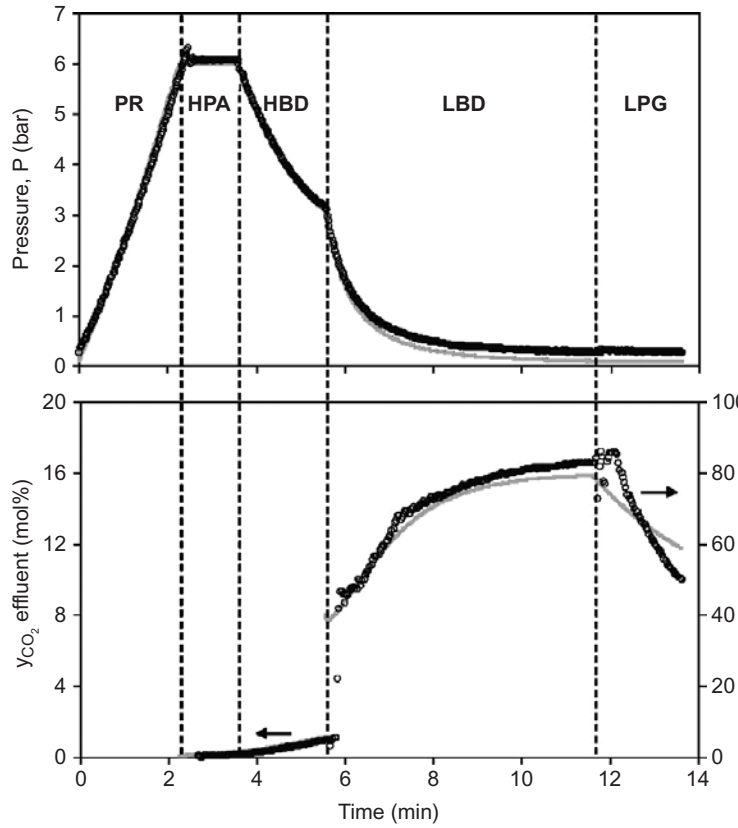

Figure 7. Illustrative comparison between the predicted (grey lines) and the experimental (black symbols) pressure and CO_2 effluent composition histories for a typical PSA run at CSS: CO_2/N_2 30:70 v/v% mixture at 309 K, P_H = 6 bar, P_L = 0.4 bar, feed flow rate of 3.0 slpm and a total feed/cycle of 10.75 ℓ STP (STP: 273 K, 1 atm).

shows both the experimental and predicted pressure, CO_2 gas-phase composition and temperature histories at CSS for the two illustrative runs. The simulated results successfully reproduce the experimental temporal profiles obtained, predicting the cyclic behaviour of both processes.

The on-line gas composition profile at column inlet was replicated experimentally by the simulated outlet streams of the membrane module. In addition to on-line monitoring of the outlet gas composition, the experimental set-up used two mass-flow controllers which fed the column with the two gases at variable flow rates. The two combined mass-flows simulated the time-varying stream that was obtained from the membrane when the hybrid process was operating under cyclic steady-state conditions. The two mass-flow rates were manipulated continuously so that the composition and mass-flow rate of the combined inlet stream were the same as those obtained for the hybrid membrane/PSA model.

Table 7 gives a more detailed comparison of the modelling results between runs A and B performed at the experimental operating conditions employed. Instead of the regular 30:70 v/v% mixture fed to the PSA, a feed stream with only 16.5% CO_2 on average was initially fed to the PSA in the hybrid process. The PR step and the first stage of the HPA were performed with a feed stream enriched in the lighter component (N_2), which was the first to be withdrawn from the column as product. This first product was then obtained at higher purity in run B (94.1% versus 84.5%).

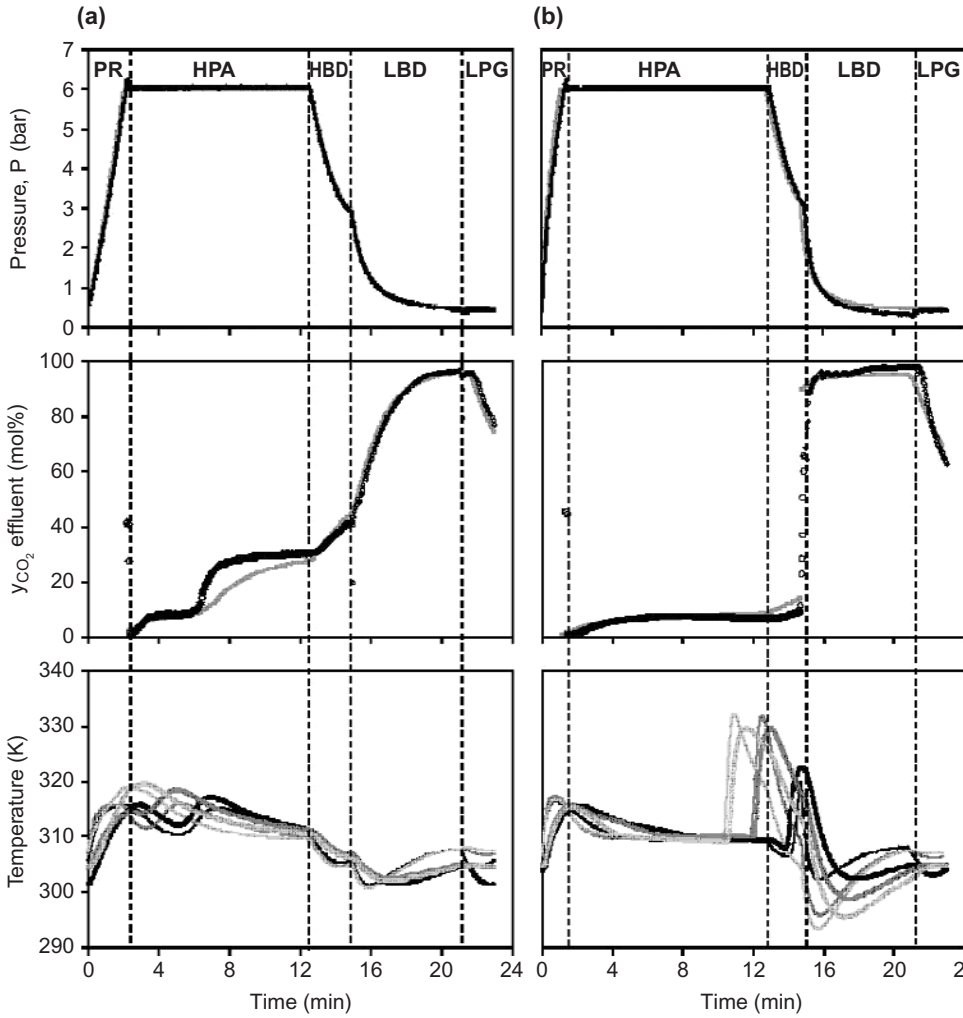

Figure 8. Experimental (symbols) and predicted (lines) pressure, CO_2 gas-phase composition and temperature (from left to right side: bottom, middle and top of the column) histories for (a) run A (simple PSA) and (b) run B (hybrid process) at CSS: CO_2/N_2 30:70 v/v% feed mixture at 309 K, P_H = 6 bar, P_L = 0.4 bar, total feed flow rate of 3.0 slpm, total feed/cycle of 40 ℓ STP (STP: 273 K, 1 atm), σ_{CO_2/N_2} = 34.4, total surface area available for permeation A_{mem} = 0.82 m^2 .

The HPA_2 step now occurred with a feed stream enriched in the more adsorbed component, simultaneously with the recovery of high purity N_2 (91.7%). The HBD step produced a purer N_2 stream than that obtained in the stand-alone PSA process. Finally, the CO_2 product was collected in the LBD and LPG steps, at a higher average purity than for the integrated case.

Depending on the membrane area available and the total amount fed into the system, the hybrid scheme (case B) enhanced the CO_2 purity and recovery up to 16% and 50%, respectively. For N_2, the respective values were 14% and 5%. Obviously, these enhancements have to be balanced with the need to compress permeate in this case, before it is fed into the PSA unit.

Figure 9 illustrates the comparison between runs A and B relative to the evolution of the CO_2 gas-phase composition during each step of the cycle, versus the axial distance z at cyclic steady

TABLE 7. Modelling Results Obtained for Run A (Single PSA) and Run B (Hybrid Process) at CSS[a]

	Run B			Run A	
Step I_1	Memb. av. CO_2 in (%)	30.21	Step I	Av. CO_2 in (%)	29.95
	Memb. total amt. in (ℓ STP)	6.711		Total amt. in (ℓ STP)	6.090
	Memb. av. CO_2 permeate out (%)	87.49			
	Memb. total amt. permeate out (%)	1.298			
	PSA av. CO_2 in (%)	16.51			
	PSA total amt. in (%)	5.413			
Step II_1	Memb. av. CO_2 in (%)	30.21	Step II	Av. CO_2 in (%)	29.95
	Memb. total amt. in (ℓ STP)	33.289		Total amt. in (ℓ STP)	31.689
	Memb. av. CO_2 permeate out (%)	85.31		Av. N_2 out (%)	84.54
	Memb. total amt. permeate out (%)	8.787		Total amt. out (ℓ STP)	26.779
	PSA av. CO_2 in (%)	10.44			
	PSA total amt. in (%)	24.502			
	PSA av. N_2 out (%)	94.14			
	PSA total amt. out (%)	22.986			
Step II_2	PSA av. CO_2 in (%)	85.59			
	PSA total amt. in (%)	10.085			
	PSA av. N_2 out (%)	91.69			
	PSA total amt. out (%)	4.789			
Step III	Av. N_2 out (%)	88.78	Step III	Av. N_2 out (%)	66.12
	Total amt. out (%)	1.662		Total amt. out (%)	3.413
Step IV	Av. CO_2 out (%)	92.99		Av. CO_2 out (%)	71.14
	Total amt. out (%)	9.564		Total amt. out (%)	6.468
Step V	Av. N_2 in (%)	97.23		Av. N_2 in (%)	97.14
	Total amt. in (%)	0.531		Total amt. in (%)	0.523
	Av. CO_2 out (%)	83.20		Av. CO_2 out (%)	87.12
	Total amt. out (%)	1.530		Total amt. out (%)	1.642
	P/F[b]	0.022		P/F[b]	0.023
Total feed per cycle[c] (ℓ STP)		40.53	Total feed per cycle[c] (ℓ STP)		38.30
CO_2 Pur (%)		91.64	CO_2 Pur (%)		74.38
N_2 Pur (%)		93.39	N_2 Pur (%)		82.19
CO_2 Rec (%)		84.13	CO_2 Rec (%)		53.31
N_2 Rec (%)		96.68	N_2 Rec (%)		92.15

[a]The feed was a 30:70 v/v% CO_2/N_2 mixture and the operating conditions reproduced the cyclic run employed experimentally. [b]Amt. of N_2 in the feed step which was consumed in the LPG step. [c]Total amt. fed per cycle to the PSA unit during PR, HPA and LPG steps.

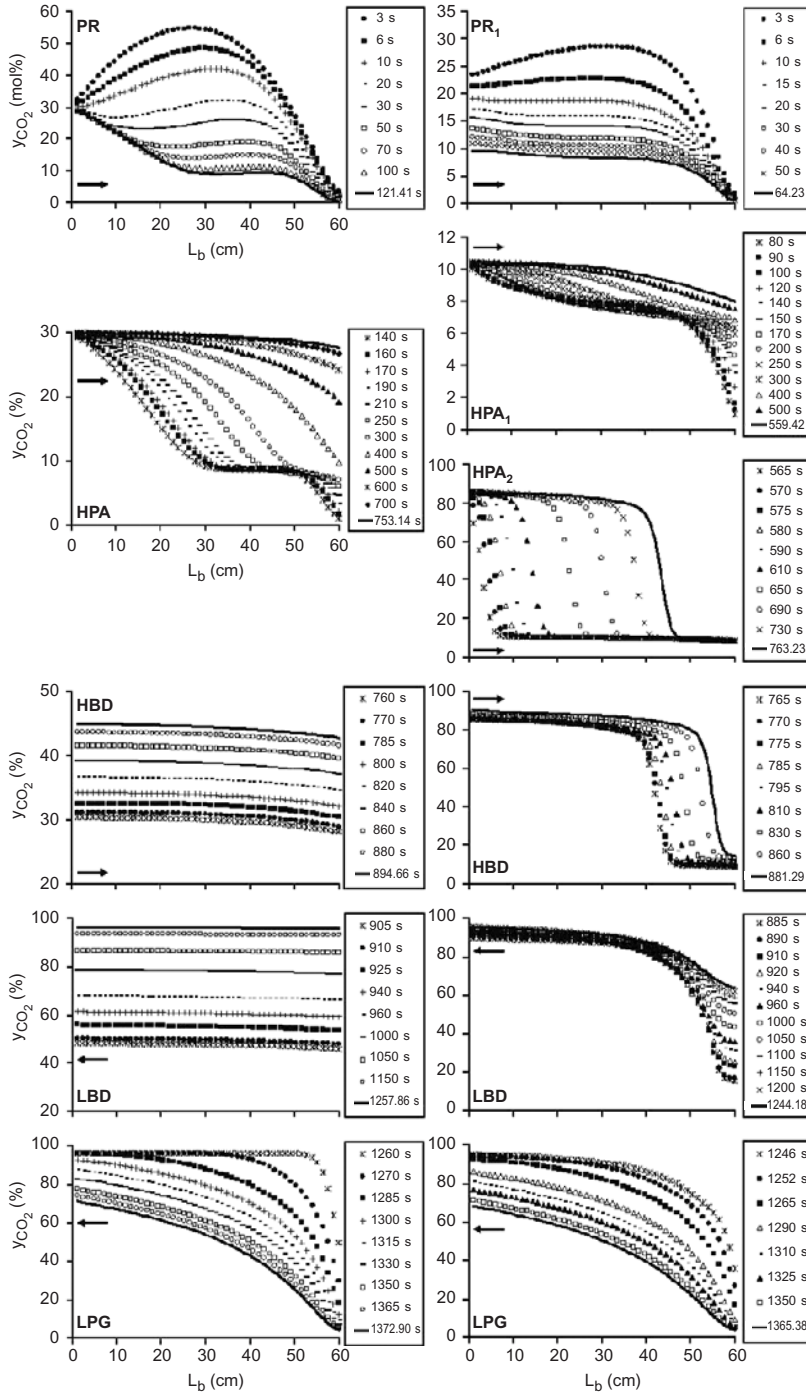

Figure 9. Carbon dioxide gas-phase composition profiles in the bed at the end of each step for (a) run A and (b) run B at CSS: CO_2/N_2 30:70 v/v% feed mixture at 309 K, P_H = 6 bar, total volumetric feed flow rate of 3.0 slpm (STP: 273 K, 1 atm). From top to bottom: $PR_1/HPA_1/HPA_2$/HBD/LBD/LPG.

state. The stiffness of the composition wave fronts inside the bed during the HPA and HBD steps is notorious for the hybrid process. Although not shown here, the temperature profiles along the bed also followed the same trend.

In order to better understand the operation of the membrane during the PR_1 and HPA_2 steps of run B, Figure 10 shows the gas composition and velocity profiles on each side of the membrane,

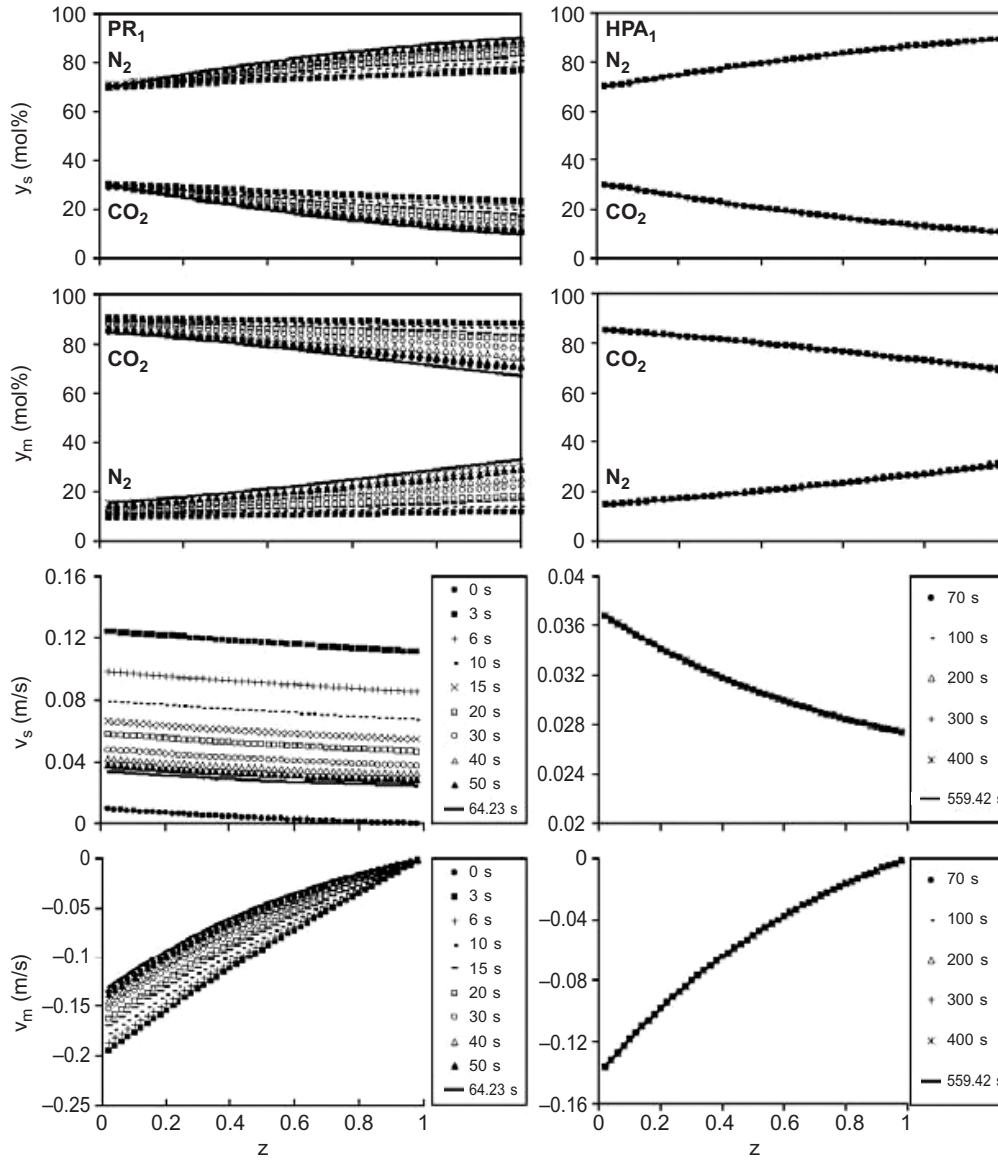

Figure 10. Evolution of the gas composition and velocity on each side of the membrane, during each step, versus the axial distance, z, for run B at CSS: CO_2/N_2 30:70 v/v% feed mixture at 309 K, P_H = 6 bar, total volumetric feed flow rate of 3.0 slpm (STP: 273 K, 1 atm).

versus the axial distance z along a CSS cycle. During permeation, the residue is enriched in the least adsorbed component, while the permeate is enriched in the more strongly adsorbed component, i.e. the more permeable species.

6. CONCLUSIONS

A novel hybrid membrane/PSA system for binary bulk gas separations has been presented and experimentally validated. Two main different hybrid cyclic schemes have been considered. A thorough model-based study was performed to assess the effect of the most important operating parameters on the performance of the system. Using the different enriched streams from the membrane, the results show that the integrated steps sharpen the composition wave fronts inside the adsorbent bed, giving rise to a decrease in band broadening and higher product purity, thereby enhancing the final process performance. This is especially evident in the high feed throughput region (Esteves and Mota 2003b; Esteves *et al*. 2004; Esteves 2005).

A five-step PSA cycle was implemented experimentally. The performance of the PSA process was predicted by simulation over a large range of operating parameters and was compared with the hybrid process. The validity of the concept was demonstrated experimentally, with both experimental and simulated results predicting an enhancement factor for the integrated membrane/PSA process over the stand-alone PSA, especially in the high feed throughput region. For the examples shown, product purities and recoveries for the hybrid process were increased by 23% and 58% for CO_2, and by 14% and 5% for N_2, compared with an equivalent stand-alone PSA.

We have shown that a pre-established PSA process, already in operation, can be eventually coupled with membrane technology giving rise to enhanced product purity and recovery. Whether these enhancements are sufficiently high to overcome the energy and investment costs for a particular separation must be determined on a case-by-case basis, supported by modelling tools and cost analysis.

ACKNOWLEDGEMENTS

This work was partly supported by FCT/MCTES through Project I&DT POCTI/EQU/ 45102/02. I.A.A.C. Esteves thanks FCT/MTCES for funding (PRAXIS XXI/BD/ 19832/99 and SFRH/BPD/ 14910/2004).

NOTATION

A	cross-sectional area of permeate and residue sides of membrane (m^2)
A_{mem}	permeation area (m^2)
b_0	parameter of Sips isotherm model (bar^{-n})
C_{pg}	heat capacity of gas [J/(mol K)]
C_{ps}	heat capacity of adsorbent [J/(kg K)]
C_{pw}	heat capacity of wall [J/(kg K)]
d_p	particle diameter (m)
D_L	axial dispersion coefficient (m^2/s)
D_h^o	stagnant bed conductivity [W/(m K)]
D_h	effective heat dispersion coefficient [W/(m K)]

e_w	wall thickness (m)
F	feed amount per cycle (ℓ STP)
F_{HPA}	reference total molar flow admitted in HPA step (mol/s)
F_m	dimensionless permeation flow parameter
FSE	Full Scale Error
h_w	wall heat-transfer coefficient [(W m^2)/K]
k_w	wall conductivity [W/(m K)]
L_b	column length (m)
L_m	membrane length (m)
n	parameter of Sips isotherm model
N	molar flux [(mol/(m^2 s)]
P	pressure (bar)
P/F	purge-to-feed ratio
Pur	purity
q	equilibrium solid loading (mol/kg)
q_m	loading at saturation (mol/kg)
Q	heat of adsorption (J/mol)
R	universal gas constant [J/(mol K)]
R_c	column radius (m)
Rec	recovery
t	time (s or min)
T	temperature (K)
v	interstitial fluid velocity (m/s)
y	mole fraction
z	axial coordinate in either the PSA bed or membrane module (m)

Subscripts

BD	counter-current blowdown
CD	co-current blowdown
d	blowdown conditions
f	feed conditions
g	purge conditions
L	low-pressure adsorption conditions
H	high-pressure adsorption conditions
HPA	high-pressure adsorption
i	component
m	permeate
p	adsorbent
PR	pressurization
PG	purge
s	residue

Greek letters

$\alpha, \beta, \gamma, \delta, \zeta$	parameters of the pressure profiles in the blowdown steps
ε	interparticle porosity

ε_p	intraparticle porosity
ρ_b	bulk density (kg/m)
ρ_p	particle density (kg/m^3)
ρ_w	wall density (kg/m^3)
τ	particle tortuosity
$\wp$	permeance, i.e., permeability divided by the active layer membrane thickness, GPU [10^{-6} cm^3 (STP) (cm^2 s cm Hg)$^{-1}$ = 3.346×10^{-5} mol/(m^2 s bar)]

REFERENCES

Alhumaizi, K. (2004) *Comput. Chem. Eng.* **28,** 1759.

Baker, R.W. (1998) *U.S. Pat. 5 785 739.*

Baker, R.W. (2002) *Ind. Eng. Chem., Res.* **41,** 1393.

Baker, R.W. and Kaaeid, K.A. (2000) *U.S. Pat. 6 011 192.*

Baker, R.W., Kaaeid, K.A., Zhenjie, H. and Pinnau, I. (2001) *U.S. Pat. 6 183 628* (to MTR Inc.).

Barton, P.I. and Pantelides, C.C. (1994) *AIChE J.* **40,** 966.

Do, D.D. (1994) *Adsorption Analysis: Equilibria and Kinetics*, Series in Chemical Engineering, Imperial College Press, London.

Domine, D. and Guerin de Montgareuil, P. (1957) *Fr. Pat. 1 223 261* (to Air Liquide Co.).

Domine, D. and Guerin de Montgareuil, P. (1964) *U.S. Pat. 3 155 468* (to Air Liquide Inc.).

Drioli, E. and Romano, M. (2001) *Ind. Eng. Chem., Res.* **40,** 1277.

Esteves, I.A.A.C. (2005) *Ph.D. Thesis*, Faculdade de Ciências e Tecnologia da Universidade Nova de Lisboa (FCT/UNL), Lisbon, Portugal.

Esteves, I.A.A.C. and Mota, J.P.B. (2002) *Desalination* **148,** 275.

Esteves, I.A.A.C. and Mota, J.P.B. (2003) "Novel Integrated Membrane/Pressure Swing Adsorption Processes for Gas Separation: A Case Study", *Proc. AIChE 2003 Annu. Meet.*, Paper 330f.

Esteves, I.A.A.C. and Mota, J.P.B. (2003) in *Adsorption Science and Technology*, Do, D.D., Ed, Imperial College Press, London, pp. 354–358.

Esteves, I.A.A.C. and Mota, J.P.B. (2005) "Gas Separation by a Novel Hybrid Membrane/Pressure Swing Adsorption Concept: Case Studies", *Proc. AIChE 2005 Annu. Meet.*, Paper 515f.

Esteves, I.A.A.C. and Mota, J.P.B. (2007) *Ind. Eng. Chem., Res.* **46,** 5723.

Esteves, I.A.A.C., Eusébio, M.F.J. and Mota, J.P.B. (2004) "Hybrid Membrane/PSA Processes for Gas Separation", *Proc. Fundamentals of Adsorption (FOA 8)*, Paper 257.

Esteves, I.A.A.C., Lopes, M.S.S., Nunes, P.M.C. and Mota, J.P.B. (2008) *Sep. Purif. Technol.*, in press.

Feng, X., Pan, C.Y., Ivory, J. and Ghosh, D. (1998) *Chem. Eng. Sci.* **53,** 1689.

Funazkri, T. and Wakao, N. (1978) *Chem. Eng. Sci.* **33,** 1375.

Haller, G.L., Fenn, J.B. and Yang, R.T. (1973) *AIChE J.***19,** 1052.

Kapantaidakis, G.C., Kaldis, S.P., Dabou, X.S. and Sakellaropoulos, G.P. (1996) *J. Membrane Sci.* **110,** 239.

Kapantaidakis, G.C., Koops, G.H. and Wessling, M. (2002) *Desalination* **145,** 353.

Karger, J. and Ruthven, D.M. (1992) *Diffusion in Zeolites and other Microporous Solids*, Wiley, New York.

Oh, M. and Pantelides, C.C. (1996) *Comput. Chem. Eng.* **20,** 611.

Patankar, S.V. (1980) *Numerical Heat Transfer and Fluid Flow,* McGraw-Hill, New York.

Ruthven, D.M., Farooq, S. and Kneabel, K.S. (1994) *Pressure Swing Adsorption*, VCH Publishers, New York.

Sircar, K.K. and Ho, W.S.W. (1992) *Membrane Handbook*, Van Nostrand Reinhold, New York.

Skarstrom, C.W. (1958) *U.S. Pat. 2 944 627* (to Esso Research & Engineering Inc.).

Sladek, K.J., Gilliland, E.R. and Baddour, A.F. (1974) *Ind. Eng. Chem., Fundam.* **13,** 100.

Strathmann, H. (2001) *AIChE J.* **47,** 1077.

Tondeur, D. (1985) *Sep. Purif. Methods* **14,** 157.

Vu, D.Q., Koros, W.J. and Miller, S.J. (2003) *Ind. Eng. Chem., Res.* **42,** 1064.
Waterson, N.P. and Deconinck, H. (1995) in *Numerical Methods in Laminar and Turbulent Flow,* Taylor, C., Durbetaki, P., Eds, Pineridge Press, Swansea, U.K., pp. 9, 203.
Wind, J.D., Paul, D.R. and Koros, W.J. (2004) *J. Membrane Sci.* **228,** 227.
Yang, R.T. (1987) *Gas Separation by Adsorption Processes*, Butterworth Publishers, Stoneham, MA, U.S.A.
Yang, R.T. and Doong, S.J. (1985) *AIChE J.* **31,** 1829.
Yang, R.T. and Doong, S.J. (1986) *AIChE J.* **32,** 397.